Numerical Simulation of Wings in Steady and Unsteady Ground Effects

A. O. Nuhait* and D. T. Mook†
Virginia Polytechnic Institute and State University, Blacksburg, Virginia

A numerical simulation of steady and unsteady ground effects is developed. The simulation is based on the general unsteady vortex-lattice method and is not restricted by planform, angle of attack, sink rate, dihedral angle, twist, crosswind, etc., as long as stall does not occur. The present computed results are generally in close agreement with limited exact solutions and experimental data. The present results show the influences of various parameters on the aerodynamic coefficients for both steady and unsteady flows. Generally, the aerodynamic coefficients increase with proximity to the ground, the greater the sink rates the greater the increases. Increasing the aspect ratio increases both the steady and unsteady ground effects for both rectangular and delta planforms. The steady ground effect increases the rolling moment and the side force. The present results serve to demonstrate the potential of the present approach.

Nomenclature

A_{ij} = normal component of the velocity generated at the control point of element i by a unit-circulation loop of vortex segments around element j
AR = aspect ratio, b^2/area; where b = span
C = root chord
C_D, C_{D_∞} = drag coefficient in and out of ground effect, respectively
C_L, C_{L_∞} = lift coefficient in and out of ground effect, respectively
C_M, C_{M_∞} = pitching-moment coefficient in and out of ground effect, respectively
C_R, C_{R_∞} = rolling-moment coefficient in and out of ground effect, respectively
C_Y, C_{Y_∞} = side-force coefficient in and out of ground effect, respectively
V_A = velocity of the wing
V_{A_X} = forward component of velocity of the wing, along the ground
V_{A_Z} = downward component of velocity of the wing
V_w = velocity induced by the wake
V_{wind} = velocity of the wind
V_∞ = apparent freestream velocity, $-(V_A - V_{\text{wind}})$, its dimensionless magnitude is one
X,Y,Z = gound-fixed coordinates
x,y,z = body-fixed coordinates
α = angle of attack $(\gamma + \theta)$, which is the angle that the wind makes with the direction of motion along the ground
γ = flight-path angle
ΔC_P = pressure jump across the lifting surface
θ = pitch angle

Introduction

DURING takeoff and landing, the aerodynamic characteristics of an airplane are influenced by the proximity of the ground. The phenomenon is called ground effect. Landing and takeoff are critical phases in a flight. As a result, extensive research, both theoretical and experimental, has been devoted to understanding and predicting ground effect. The first basic theory was developed by Wieselsberger[1] in 1922. He placed an image of the real wing below the ground plane. Then he used the basic concepts of the lifting-line theory of Prandtl to calculate a correction, which was used to modify the classical induced drag and induced angle of attack of wings out of ground effect. The theory ignores the effect of the bound vortex in the image.

Since then, almost all investigators have employed the image concept to simulate the ground effect with the wing height fixed in time (a situation that may be called steady ground effect) and the wake position assigned. This model has two shortcomings: first, the wake deforms and rolls up into the force-free position, and second, during a landing and takeoff the height is changing and hence the flow is unsteady. Indeed, for some military applications the height can change very rapidly. In 1985, Chen and Schweikhard[2] obtained the unsteady ground effect in the case of a two-dimensional flat plate, assuming the wake to be straight along the flight path. They eliminated one shortcoming, but they still assigned the position of the wake and they did not have the capability of studying the effects of aspect ratio. They began the unsteady simulation by first obtaining the steady state at a given height and then having the plate descend along a straight flight path. They found that the increase in lift for unsteady ground effect is greater than the increase for steady ground effect for intermediate heights above the ground. This effect is reversed when the airfoil is very close to the ground where the influence of the shed vortices becomes more prominent. They speculated that a similar trend of lift variations exists in the case of a finite wing. Between 1985 and 1987, Chang[3] and Chang and Muirhead[4,5] tested several thin, flat, delta wings in both steady and unsteady ground effects.

In 1985, Katz[6] used a vortex-lattice method that included a freely deforming wake to investigate the performance of lifting surfaces close to the ground, such as those found on racing cars. Katz found that the increases in aerodynamic loads due to the unsteady ground effect are about 100% greater than those due to the steady ground effect.

In the present paper, a general model of finite lifting surfaces in steady and unsteady ground effect is developed. The present method is an extension of the general unsteady vortex-lattice method published by Konstadinopoulos et al.[7] in 1985. The present method is not restricted by planform, camber, twist, dihedral angle, sink rate, angle of attack, etc., as long as separation occurs only along known lines and vortex bursting

Presented as Paper 88-2546 at the AIAA 6th Applied Aerodynamics Conference, Williamsburg, VA, June 6-8, 1988; received Nov. 7, 1988; revision received May 26, 1989.

*Graduate Student, Department of Engineering Science and Mechanics; currently at King Saud University, Saudi Arabia.
†Professor, Department of Engineering Science and Mechanics. Member AIAA.

does not occur near the lifting surface. Moreover, the flight path is not restricted to a straight line. The present method can be used to investigate the effect of both steady and unsteady ground effects.

Method of Approach and Numerical Examples

The flow is incompressible and inviscid and separates only along the trailing edges and wing tips, or leading edges in the case of highly swept delta wings. Following Wieselsberger, we add the image of the wing and its wake below the ground and thereby make the ground a plane of symmetry. If the ground is rough and not to be modeled as a plane, then one can omit the images and instead place panels on the ground.

The lifting surface is divided into panels or elements; a typical arrangement is shown in Fig. 1a. The solid lines represent discrete vortex segments, and the two broken lines represent the trailing and leading edges. In the figure, the wing is advancing toward the top of the page. The offset at the leading and trailing edges follows the so-called one-quarter-three-quarter chord rule. The offset does nothing to the values of the predicted force, but improves the accuracy of the predicted moments. The small crosses are the so-called control points—the points where the no-penetration condition is imposed:

$$(V - V_{LS}) \cdot n = 0 \tag{1}$$

at each control point. In Eq. (1), V is the velocity of the fluid particle in contact with the control point and V_{LS} is the velocity of the control point, which is considered part of the lifting surface.

Each element is enclosed by a quadrilateral ring of finite discrete vortex segments. The circulations around all of the segments in a given ring are the same; consequently, circulation is spatially conserved. The velocity field generated by such a ring is computed by repeated applications of the Biot-Savart law; consequently, the velocity field satisfies the continuity equation and decays as the reciprocal of the distance from the segment.

The velocity of the control point is computed according to the relationship for a rigid body:

$$V_{LS} = V_A + \Omega \times r \tag{2}$$

where V_A is the velocity of the origin of a moving reference frame (point A) that is attached to the wing, Ω the angular velocity of the moving reference frame, and r the position of the control point relative to the moving reference frame.

In general, the spatial orientation of the wing is given by a set of Euler angles. Derivatives of the Euler angles can be specified and used to compute Ω. In the present paper, $\Omega = 0$.

The problem is posed in terms of the moving reference frame; consequently, Bernoulli's equation must be modified:

$$2\left[\frac{\partial \phi}{\partial t} - V \cdot (V_A + \Omega \times r)\right] + V^2 + \frac{2p}{\rho} = \frac{2p_\infty}{\rho} + V_\infty^2 \tag{3}$$

where $\partial\phi/\partial t$ is the derivative of the velocity potential at a fixed position in the moving reference frame, p the pressure, and ρ the density (necessarily a constant).

In the present simulation, the wing moves through the air. Typically, V_∞ is taken to be zero. An exception is the case of wind for which V_∞ may be considered a function of time, changing both magnitude and direction.

To obtain the loads, the difference in the pressure across the lifting surface is computed at each control point, the difference is multiplied by the area of the element to produce the force on the element, the elemental forces and their moments are added, and the resultants are resolved into lift, drag, pitching moment, etc.

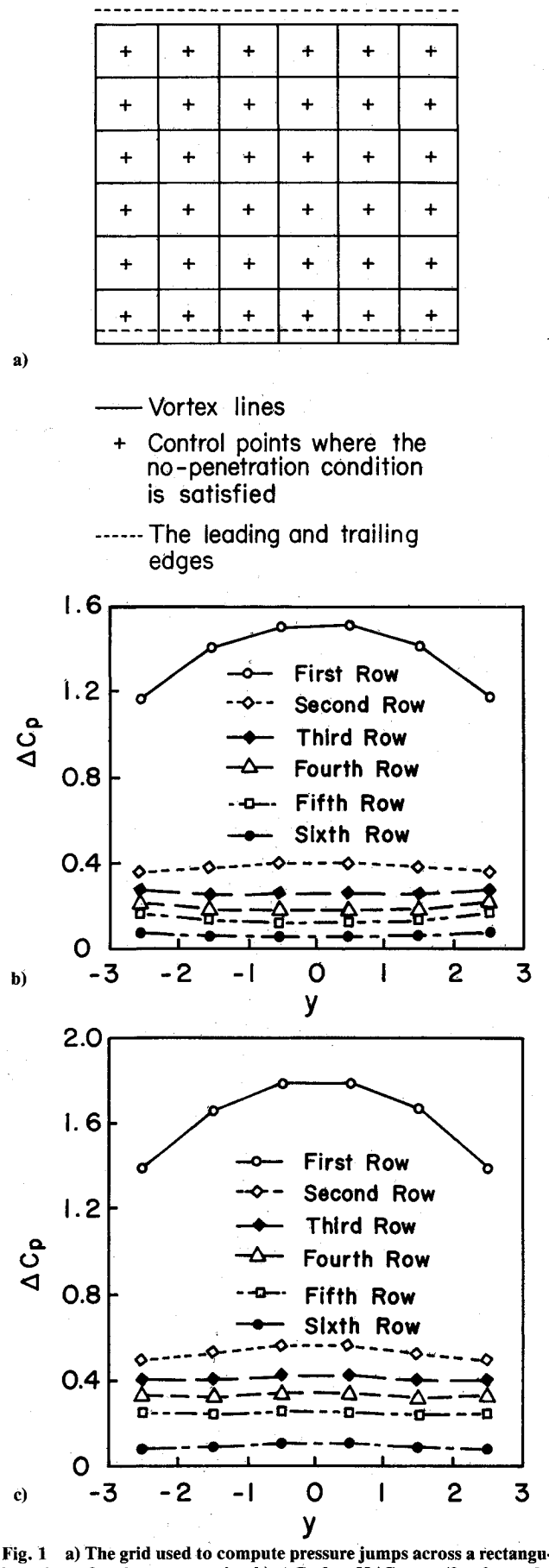

Fig. 1 a) The grid used to compute pressure jumps across a rectangular wing of unit aspect ratio; b) ΔC_p for $H/C = \infty$ (far from the ground); and c) ΔC_p for $H/C = 0.16$ at $\alpha = 10$ deg, where H is the height of the trailing edge above the ground, and ΔC_p is the dimensionless pressure coefficient.

At each control point, the pressure jump is computed according to the following expressions:

$$\Delta p = p_\ell - p_u = -p\left[\frac{\partial G}{\partial t} + \Delta V \cdot (V - V_A - \Omega \times r)\right] \quad (4)$$

where p_ℓ and p_u are the pressures on the lower and upper surfaces, G the circulation around the vortex segments in the ring enclosing the control point, and ΔV the local jump in velocity across the lifting surface. The derivative of G is computed according to a finite-difference formula. The ΔV is computed by assuming that the circulations around the vortex segments represent the average vorticity in the direction of the segment times a thickness (i.e., a dimension perpendicular to the surface) times the distance between the two segments. (The concept is that the thickness vanishes while the magnitude of the vorticity increases in such a way that the product of vorticity and thickness remains constant.) The component of the velocity jump perpendicular to the segments is the average vorticity times the "thickness." As before, V is the velocity induced by all of the vortex segments representing the lifting surface (wing) and its wake.

In Figs. 1b and 1c, the pressure difference across the lifting surface is plotted for the mesh shown in Fig. 1a. The points are where the calculation was actually made, the control points of the mesh. In Fig. 1b, the wing is out of ground effect, and in Fig. 1c, the wing is close to the ground. Each line in the plot shows the spanwise variation of the pressure difference along a constant position of chord. The foremost line resembles the variation predicted by classical lifting-surface theories. The variations in the midchord region show the effect of the wing-tip vortex systems. For the aftmost position where the control points are nearest the trailing edge, the predicted difference is very small in accord with the Kutta condition. Along the wing tips, the predicted pressure jump differs from zero noticeably; the actual pressure difference drops very sharply to zero here. When a sufficient number of elements are used, the present approach predicts the sudden pressure drop better. The present numerical treatment of the Kutta condition is discussed below. By comparing Figs. 1b and 1c, one can see how the ground effect alters the pressure distribution. Below we consider the effect of the ground on gross aerodynamic coefficients such as lift, drag, etc.

Before going to a discussion of the results, we explain how the wake is generated. As an example, we consider the case of an impulsive start. The first step is to compute the influence matrix A_{ij}, where A_{ij} is the normal component of the velocity at the control point of element i generated by unit circulation around the vortex segments enclosing element j and its image. At the start of the motion, the no-penetration condition [Eq. (1)] becomes

$$\sum_{j=1}^{N} A_{ij} G_j = (V_{LS} \cdot n)_i \quad (5)$$

for $i = 1, 2, \ldots, N$, where N is the total number of elements, and G_j is the circulation around the vortex segments enclosing element j. When the flight path is inclined to the ground and/or the wing is deforming, the influence coefficients must be recomputed at each time step. After the G_j are found, one convects the segments along the edges where the so-called Kutta condition is to be imposed. To eliminate a pressure jump around a vortex segment, we convect it at the local particle velocity (that is, we enforce the condition $D\Gamma/Dt = 0$, sometimes referred to as the temporal conservation of vorticity). Specifically, we compute the velocities at both ends of the segments and then displace the ends according to the following formula:

$$\Delta r = (V - V_A - \Omega \times r)\Delta t \quad (6)$$

where Δr is the displacement in the moving frame and Δt is the time step. We have experimented with more accurate algorithms, but found this simple one to be adequate. In the present example, all of the segments along the wing tips and trailing edges are "shed" and convected away from the wing. To maintain temporal conservation of circulation, each entire quadrilateral element is shed into the wake, one row of elements at each time step; thus, the wake is generated step by step. The circulations around the vortex segments in the wake are known from the imposition of the no-penetration condition at previous time steps. Actual computed wakes are shown in Fig. 2. In Fig. 2b, the position of the ground is shown for reference.

When there is a crosswind, the wing-tip wake on the windward side is blown inboard while the one on the leeward side is blown outboard and symmetry is destroyed.

After the first time step, Eq. (5) must be modified:

$$\sum_{j=1}^{N} A_{ij} G_j = (V_{LS} - V_w) \cdot n_i \quad (7)$$

where V_w is known from the calculations made at previous times.

Steady-state results are obtained by giving the wing an impulsive start and having it move forward at constant velocity until the steady state develops.

In the case of unsteady ground effect, we initially located the wing far from the ground, so that the flow would reach a

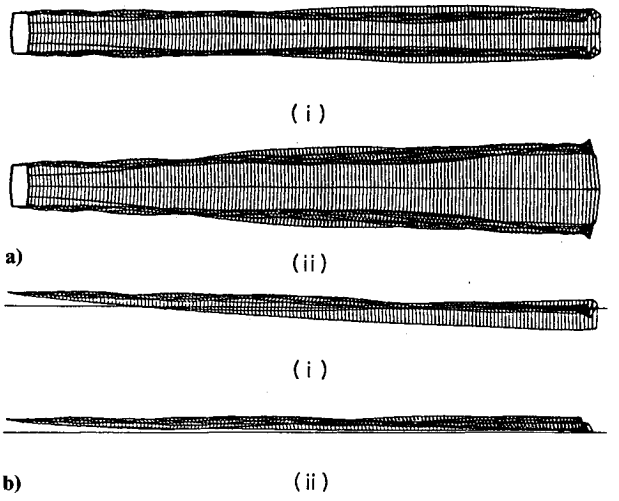

Fig. 2 Actual computed wakes for a low-aspect-ratio, tapered wing ($AR = 1.9$) in and out of ground effect for steady flow: a) top views for (i) out of ground effect and (ii) in ground effect; and b) side views for (i) out of ground effect and (ii) in ground effect, $\alpha = 10$ deg.

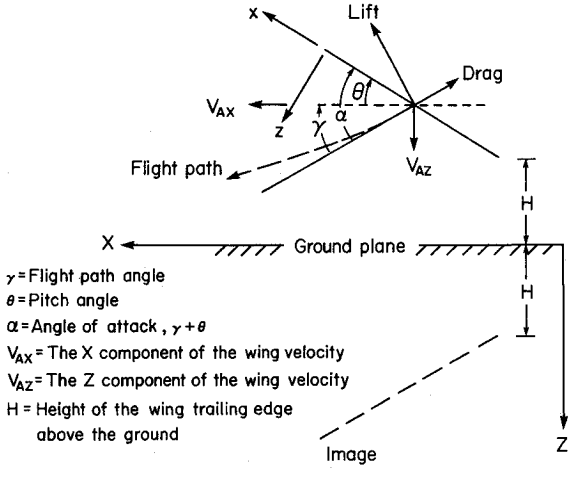

Fig. 3 A side view of a wing and its image near the ground.

steady state while the wing descends along the flight path before it experiences the ground effect. For the computations, we varied the sink rates by varying the flight-path angle γ. In Fig. 3, a wing and its image near the ground are represented schematically. The definitions of the flight-path and pitch angles and how they are related to the angle of attack are shown. The flight-path angle is related to the velocity of the wing by the following:

$$\gamma = \tan^{-1} \frac{V_{A_Z}}{V_{A_X}} \tag{8}$$

We often refer to γ as the sink rate. The apparent freestream velocity V_∞ is given by

$$V_\infty = -(V_A - V_{\text{wind}}) \tag{9}$$

The wind velocity is parallel to the ground plane and makes an angle η with the direction of forward motion. All of the results, except those in Fig. 12, are computed with $V_{\text{wind}} = 0$.

Comparisons of Exact Solutions and Present Results

As a means of establishing the credibility of the vortex-lattice technique, we use it to predict the steady ground effect for two-dimensional circular-arc airfoils with various cambers. The results are compared with an exact solution found by Tomotika et al.[8] in 1951. The exact solution and the computed lift and pitching-moment (about the trailing edge) increments are plotted as functions of height above the ground in Fig. 4. The angle of attack is always 5 deg. The results for the flat plate (zero camber) are given in Fig. 4a. The agreement is excellent. The results for the circular-arc airfoil with 0.053 camber are shown in Fig. 4b. For camber, the agreement is excellent also. The effect of the ground on the lift and moment of an airfoil is greatly modified by its camber. For moderate camber, the ground effect first lowers the lift and moment and then raises them as the airfoil approaches the ground. For larger camber, there is essentially only a loss in lift and moment.

The vortex-lattice method is not restricted to two-dimensional steady flows, as is the analysis of Tomotika et al. Below, we consider wings of finite aspect ratio in steady and unsteady ground effect.

Comparisons of Present and Experimental Results for the Wing of an F-104A

In Fig. 5, the aerodynamic coefficients in and out of ground effect are plotted. In each plot the results computed by the

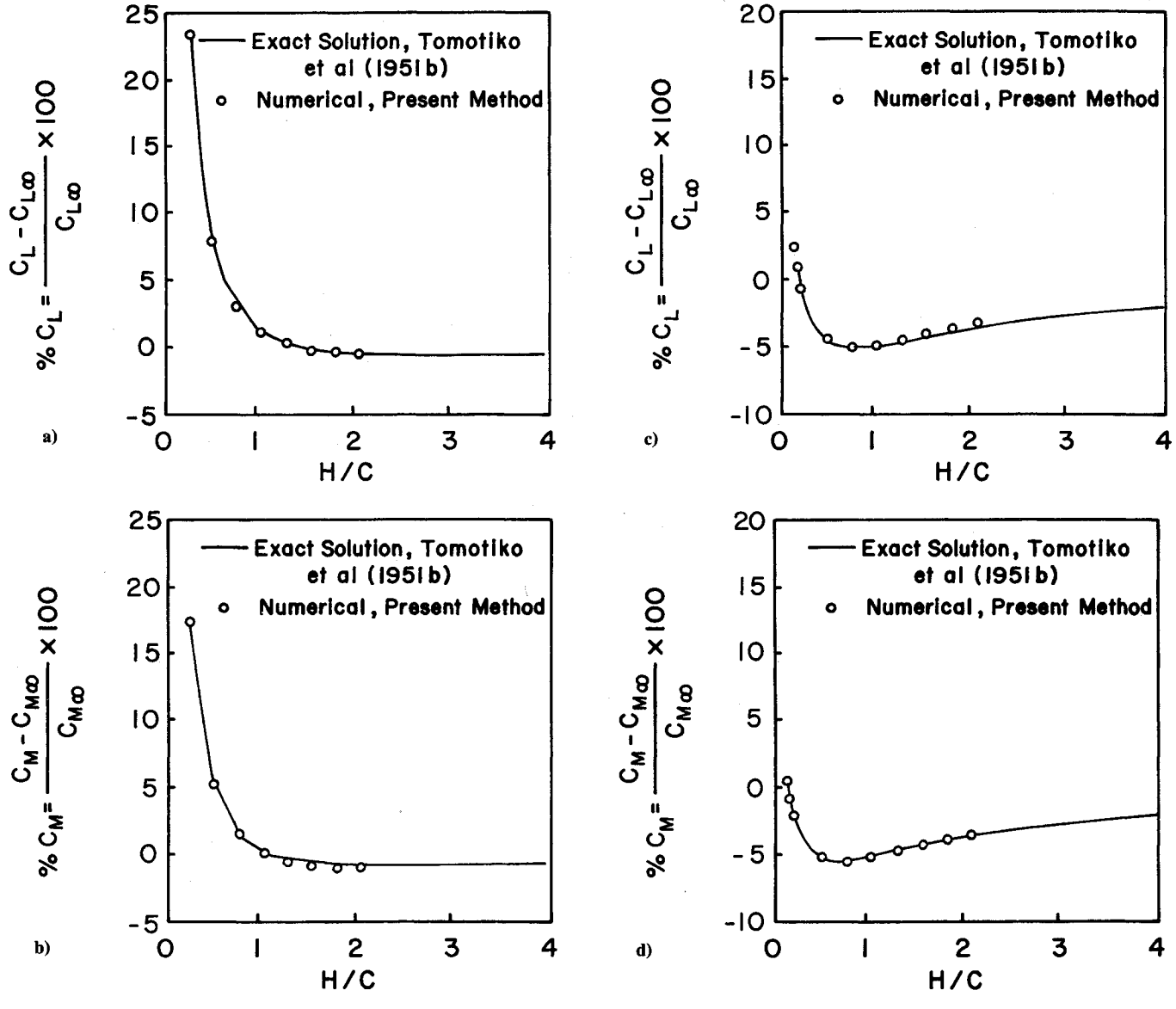

Fig. 4 A two-dimensional flat plate in steady ground effect: a) lift and b) pitching-moment (about the trailing edge) coefficients as functions of height of the trailing edge above the ground at $\alpha = 5$ deg. A two-dimensional circular-arc airfoil (camber = 0.053) in steady ground effect: c) lift and d) pitching-moment (about the trailing edge) coefficients as functions of height of the trailing edge above the ground at $\alpha = 5$ deg.

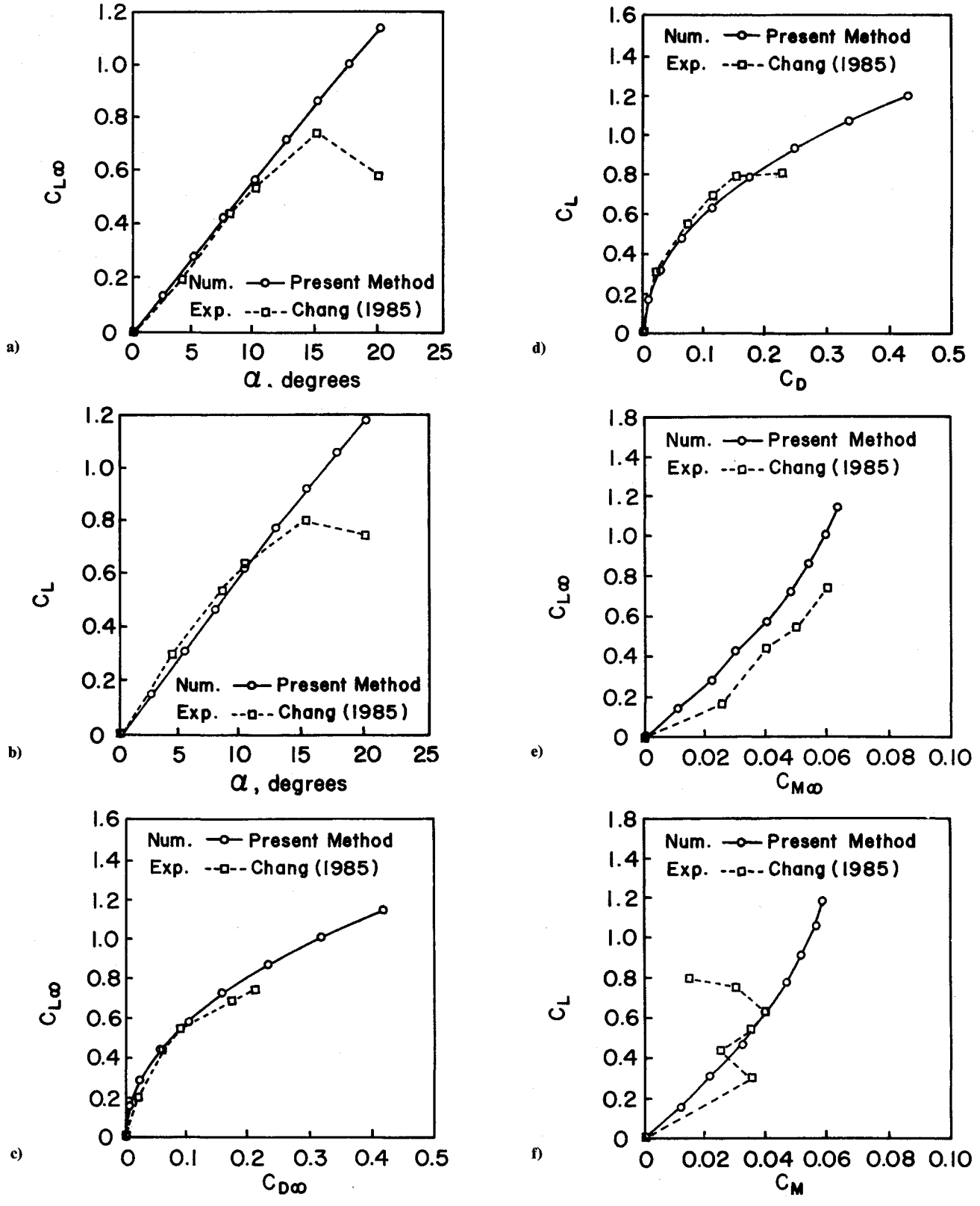

Fig. 5 A comparison of the computed and experimental results in steady flow for an F-104A wing: a) and b) lift coefficients out of and in ground effect as functions of angle of attack, respectively; c) and d) lift coefficients out of and in ground effect as functions of drag coefficients, respectively; e) and f) lift coefficients out of and in ground effect as functions of pitching-moment coefficients, respectively. For the case near the ground, $h/b = 0.28$, where h is the height above the ground of a point 0.55 chord behind the apex.

present method are compared with experimental data. The height above the ground divided by the span (h/b) is equal to 0.28 for the case near the ground, where h is measured to a point 0.55 chord behind the apex. In Figs. 5a and 5b, the lift coefficients out of and in ground effect, respectively, are given as functions of angle of attack. The agreement is good up to approximately 10 deg angle of attack. Beyond 10 deg, the data seem to show stall occurring in both cases. In Figs. 5c and 5d, lift coefficients are plotted as functions of the drag coefficients for out of and in ground effect, respectively. Both plots show good agreement with experimental results. In Figs. 5e and 5f, the lift coefficients are plotted as functions of pitch-

ing-moment coefficients far from the ground. The trends for both curves are the same. Near the ground, Fig. 5f, there seems to be a problem with the experimental data.

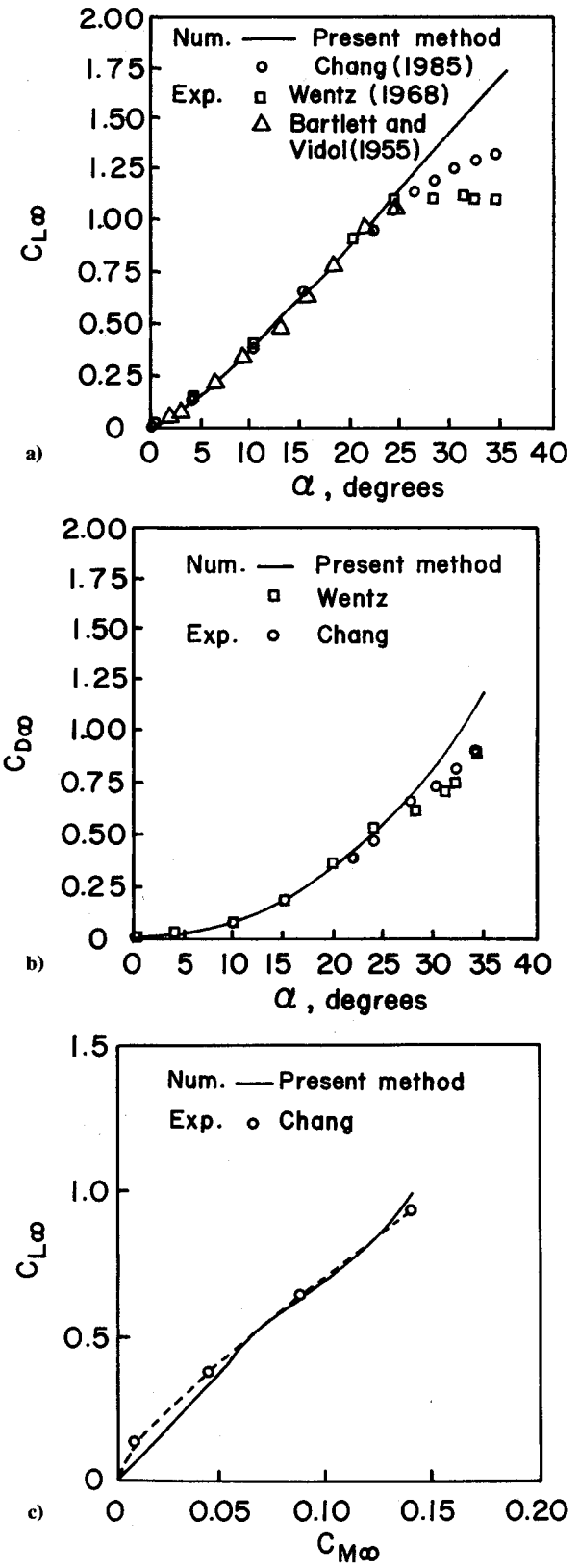

Fig. 6 Numerical and experimental results for a thin, flat, delta wing of aspect ratio 1.456 out of ground effect for steady flow: a) lift coefficient as a function of angle of attack; b) drag coefficient as a function of angle of attack; and c) pitching-moment coefficient about an axis passes through the apex, based on the root chord, as a function of angle of attack.

Delta Wings

In Fig. 6, the computed and experimental aerodynamic coefficients are plotted as functions of the angle of attack far from the ground. The experimental results are taken from Bartlett and Vidal,[9] Chang,[3] and Wentz.[10] The wing is a flat, thin, delta wing with a sweepback angle to 70 deg ($\mathcal{A}R = 1.456$). The pitching moment was calculated about the axis through the apex. The coefficient is based on the root chord. There is good agreement between the computed and experimental results up to approximately 25 deg angle of attack where stall begins.

In Fig. 7, the changes in the coefficients of lift and drag for steady flow are plotted as functions of the height of the trailing edge above the ground for a thin, flat, delta wing ($\mathcal{A}R = 1.456$) at 22.1 deg angle of attack. The computed lift and the experimental data of Chang are in good agreement. For drag, both sets of results show the same trend, but they do not agree as well as those for lift.

In Fig. 8, the changes in the coefficients of lift for unsteady flow are plotted as functions of the height of the midpoint of the root chord above the ground for a thin, flat, delta wing ($\mathcal{A}R = 1.456$) at 22.1 deg angle of attack. The results for steady flow are included for comparison. The computed lift and the experimental data of Chang are in fair agreement.

When H (the height of the midpoint of the root chord) is fixed and the flight-path is rotated downward, h (the height of

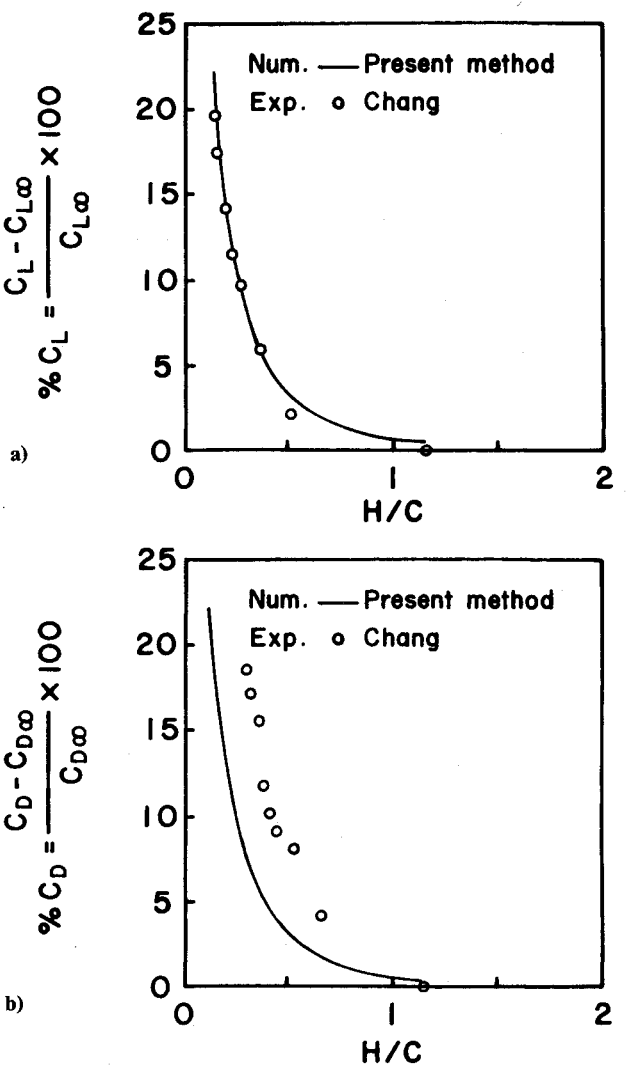

Fig. 7 A comparison of the computed and experimental results for a delta wing of aspect ratio = 1.456 in steady ground effect: a) lift and b) drag increments at $\alpha = 22.1$ deg as functions of the height of the trailing edge above the ground.

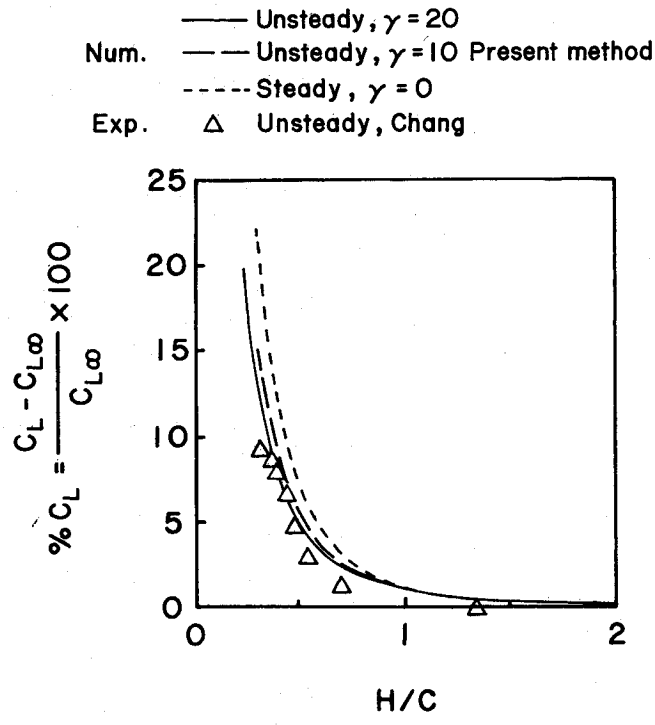

Fig. 8 A comparison of the computed and experimental results for a delta wing of aspect ratio = 1.456 in unsteady ground effect: lift increments at $\alpha = 22.1$ deg as functions of the height of the midpoint of the root chord above the ground.

the trailing edge at the root chord) increases. For a given *H*, the aerodynamic coefficients decrease as the flight-path angle increases. However, as the next set of results show, for a given *h*, the aerodynamic coefficients increase as the flight-path angle increases. Before one can state a trend, it must be clear which height is used. Here, we use the trailing-edge height unless we state otherwise.

In Fig. 9, the changes in the aerodynamic coefficients are plotted as functions of the height of the trailing edge above the ground for different sink rates. The wing is a flat, thin, delta wing ($AR = 1.456$) at 22.1 deg angle of attack. It is clear that the ground effect increases all coefficients and the effect is stronger at higher sink rates.

In Fig. 10, the changes in the aerodynamic coefficients for a thin delta wing are plotted as functions of the height of the trailing edge above the ground for different aspect ratios for unsteady ($\gamma = 20$) flow. The angle of attack is 10 deg. The ground effect increases the coefficients and the effect is stronger for larger aspect ratios.

Rectangular Wings

In Fig. 11, the changes in the aerodynamic coefficients are plotted as functions of the height of the trailing edge above the ground for different sink rates for a rectangular wing. The angle of attack is 10 deg and the aspect ratio is unity. The proximity of the ground increases all of the aerodynamic coefficients, and the effect is stronger for higher sink rates. This trend was also noticed for aspect ratios of 2 and 4. The trend is stronger for larger aspect ratios.

In Fig. 12, plots of the changes in rolling moment and side force for a rectangular wing of unit aspect ratio at 10 deg angle of attack and 5 deg roll for steady flow are plotted as functions of the height of the trailing edge above the ground. The magnitude of the wind velocity is taken to be 10% of the magnitude of the velocity of the wing. In this example, the wind velocity is parallel to the ground and at 20 deg with the flight path. The ground effect increases the rolling moment and side force.

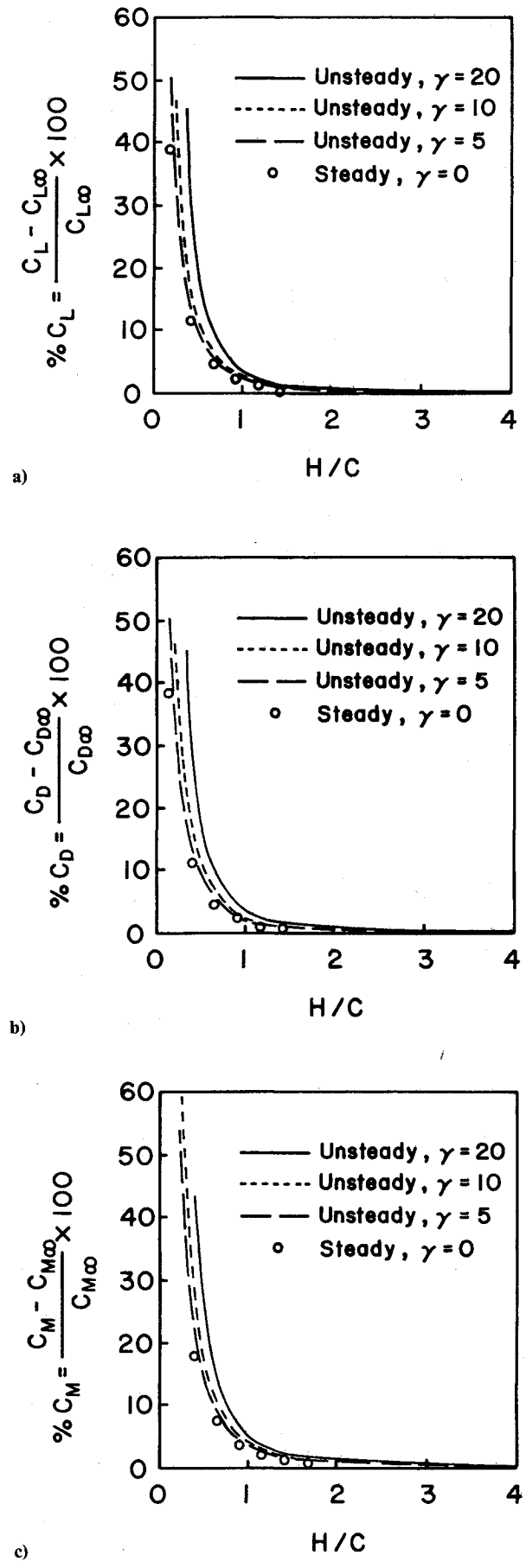

Fig. 9 Computed results for a delta wing of aspect ratio 1.456 in ground effect: a) lift; b) drag; and c) pitching-moments at $\alpha = 10$ deg as functions of the height of the trailing edge above the ground for different sink rates.

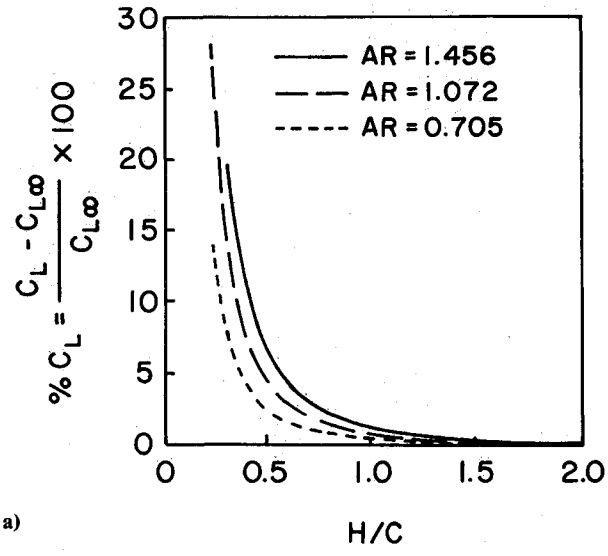

a)

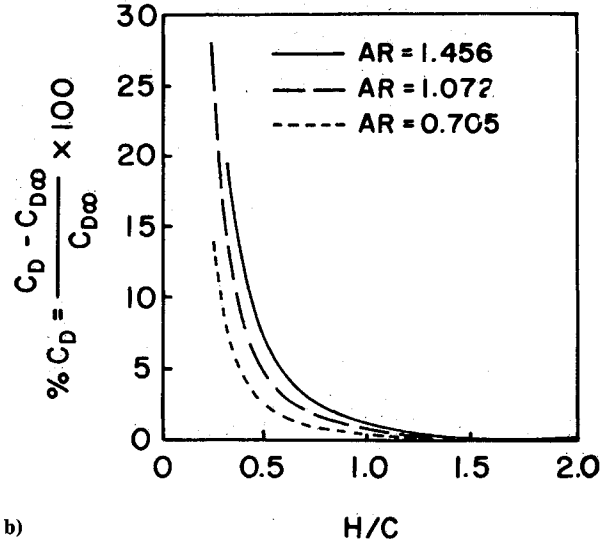

b)

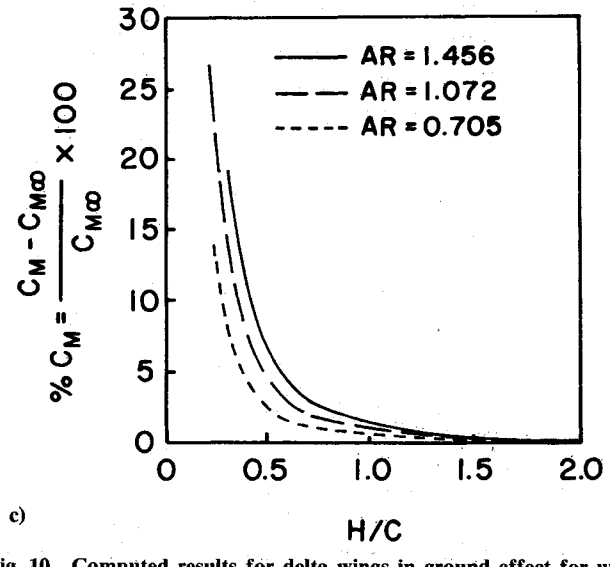

c)

Fig. 10 Computed results for delta wings in ground effect for unsteady flow: a) lift; b) drag; and c) pitching-moments increments at $\alpha = 10$ deg and $\gamma = 20$ deg as functions of the height of the trailing edge above the ground for different aspect ratios.

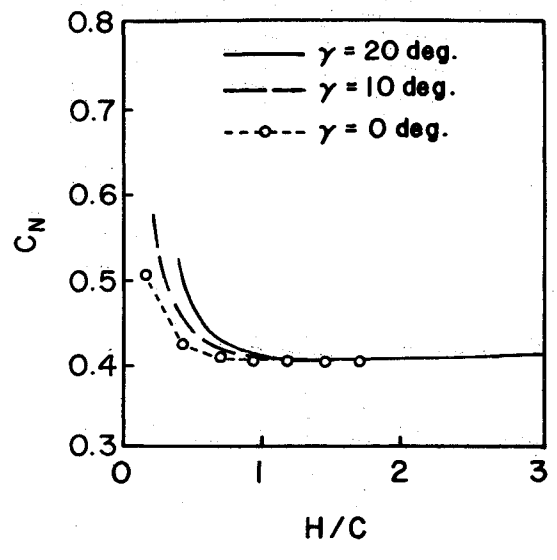

a)

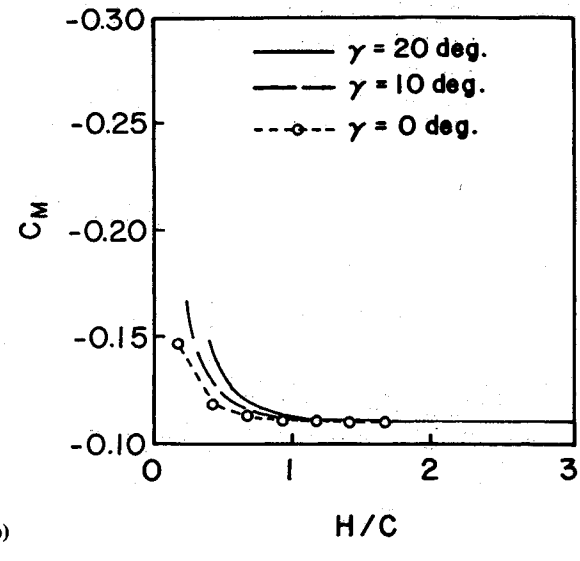

b)

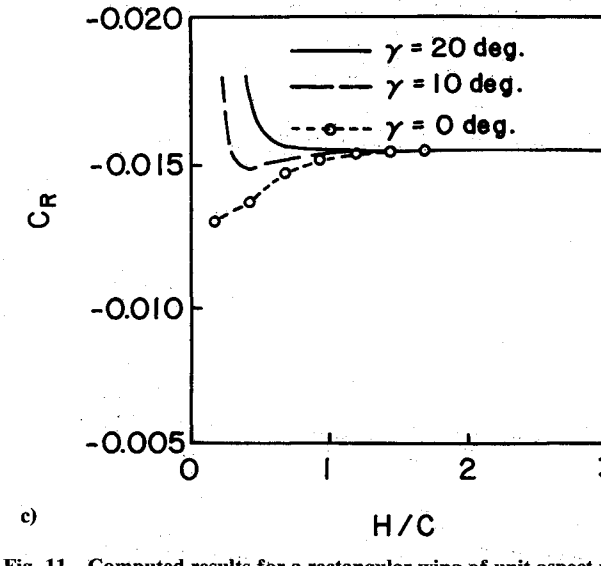

c)

Fig. 11 Computed results for a rectangular wing of unit aspect ratio in ground effect: a) lift; b) drag; and c) pitching-moment increments as functions of the height of the trailing edge above the ground for different sink rates. $\alpha = 10$ deg.

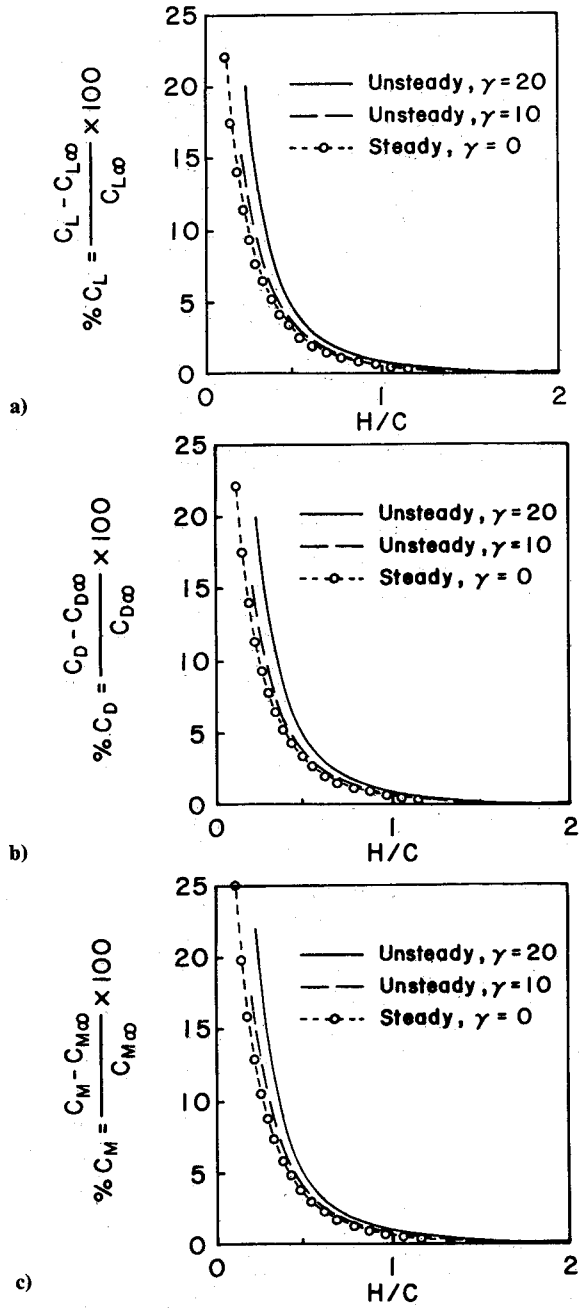

Fig. 12 Computed results for a rectangular wing of aspect ratio in ground effect with crosswind: a) normal-force; b) unit pitching-moment; and c) rolling-moment coefficients, at $\alpha = 10$ deg, $\phi = 5$ deg and 10% crosswind velocity at 20 deg, as functions of the height of the trailing edge above the ground for different sink rates.

Conclusion

The present simulation of the ground effect predicts higher aerodynamic coefficients (when the coefficients are considered functions of the height of the trailing edge) for unsteady cases than for steady cases; the greater the sink rate the stronger the effects. These effects are observed for both rectangular and delta wings. Increasing the aspect ratio increases the ground effects for rectangular and delta wings in both steady and unsteady flows. The effect of the ground also increases the rolling moment and side force.

Although the present results are for straight flight paths, the present approach can be used to simulate any prescribed flare. The present approach can also be extended to model steady and unsteady aerodynamic interference among multiple, closely coupled lifting surfaces.

Acknowledgment

This work was partially supported by the Air Force Office of Scientific Research under Grant AFOSR-85-0158.

References

[1]Wieselsberger, C., "Wing Resistance Near the Ground," NACA TM 77, 1922.

[2]Chen, Y.-S. and Schweikhard, W. G., "Dynamic Ground Effects on a Two-Dimensional Flat Plate," *Journal of Aircraft,* Vol. 22, July 1985, pp. 638–640.

[3]Chang, R. C., "An Experimental Investigation of Dynamic Ground Effect," Ph.D. Dissertation, Dept. of Aerospace Engineering, Univ. of Kansas, Lawrence, KS, April 1985.

[4]Chang, R. C. and Muirhead, V. U., "Investigation of Dynamic Ground Effect," NASA CP-2462, 1985.

[5]Chang, R. C. and Muirhead, V. U., "Effect of Sink Rate on Ground Effect of Low-Aspect-Ratio Wings," *Journal of Aircraft,* Vol. 24, March 1987, pp. 176–180.

[6]Katz, J., "Calculation of the Aerodynamic Forces on Automotive Lifting Surfaces," *Journal of Fluid Engineering,* Vol. 107, Dec. 1985, pp. 438–443.

[7]Konstadinopoulos, P., Thrasher, D. F., Mook, D. T., Nayfeh, A. H., and Watson, L., "A Vortex-Lattice Method for General Unsteady Aerodynamics," *Journal of Aircraft,* Vol. 22, Jan. 1985, pp. 43–49.

[8]Tomotika, S., Tamada, K., and Umemoto, H., "The Lift and Moment Acting on a Circular-Arc Aerofoil in a Stream Bounded by a Plane Wall," *Quarterly Journal of Mechanics and Applied Mathematics,* Vol. 4, Jan. 1951, pp. 1–22.

[9]Bartlett, G. E. and Vidal, R. J., "Experimental Investigation of the Influence of Edge Shape on the Aerodynamic Characteristics of Low-Aspect-Ratio Wings at Low Speeds," *Journal of the Aeronautical Sciences,* Vol. 22, Aug. 1955, pp. 517–533, 588.

[10]Wentz, W. H., "Wind-Tunnel Investigation of Vortex Breakdown on Slender Sharp-Edge Wings," Ph.D. Dissertation, Univ. of Kansas, Lawrence, KS, 1968.